

Expansion of 1D polarized superfluids: The FFLO state reveals itself

Hong Lu¹, L. O. Baksmaty¹, C. J. Bolech^{2,1}, and Han Pu¹

¹*Department of Physics and Astronomy, Rice University, 6100 Main street, MS-61, Houston, TX 77005.*

²*Department of Physics, University of Cincinnati,
345 Clifton Court, ML-11, Cincinnati, OH 45221-0011.*

(Dated: July 22, 2018)

We study the expansion dynamics of a one dimensional polarized Fermi gas after sudden release from confinement using both the mean-field Bogoliubov-de Gennes and the numerically exact Time-Evolving Block Decimation methods. Our results show that experimentally observable spin density modulations directly related to the presence of a Fulde-Ferrel-Larkin-Ovchinnikov (FFLO) state develop during the expansion of the cloud, providing incontrovertible evidence of this long-sought state.

PACS numbers: 67.85.-d, 03.75.Ss, 37.10.Gh, 71.10.Fd

Since the introduction of the Bardeen-Cooper-Schrieffer (BCS) theory, physicists have speculated on the fate of the superconducting pairing correlation in the presence of a polarizing effect. This could arise from a mass imbalance of the pairing fermions such as in color superconductivity or in the vicinity of magnetic impurities within conventional superconductors. The FFLO (Fulde-Ferrel-Larkin-Ovchinnikov) [1–3] proposal suggests that in such circumstances the condensation will occur from pairs with finite center-of-mass momenta. Despite decades of work [4–6], this state has not been unambiguously observed. Although recent experiments [7] in one dimension (1D) confirmed important aspects of the phase diagram [8, 9], conclusive evidence of the FFLO phase was not obtained. We show here that during a non-equilibrium expansion, the polarized 1D superfluid develops strong signatures in the density profiles of the pairing species which are a direct consequence of the FFLO crystalline order and constitute incontrovertible evidence.

We focus on a polarized degenerate Fermi gas confined to a 1D harmonic trap. In general, according to the Mermin-Ho-Wagner theorem, a 1D superfluid system cannot support superfluidity and would possess, at best, algebraically decaying long range order at zero temperature ($T = 0$). However for the finite systems that we study here, there is copious theoretical evidence that FFLO correlations occur and are fairly robust [10–17]. We also note that the experiments use not a single 1D trap but a loosely coupled array which allows tuning of the inter-tube coupling and thus makes it possible to study the 3D to 1D crossover physics [7]. Although a partially polarized phase was observed through direct imaging in the experiment, it is quite clear from recent work that the FFLO correlations *do not* leave a detectable signature on the ground state density profiles. Thus the character of the partially polarized phase remains unknown.

We consider a gas of N fermionic particles each of mass m with two spin projections labeled by $\sigma = (\uparrow, \downarrow)$ confined to a cigar-shaped harmonic trap. Consistent with experimental reality [7, 18–22], we assume that the inter-particle interaction arises from a broad fesh-

bach resonance and is amenable to exquisite control. In these systems, the ratio of the radial ω_r and axial ω_z trapping frequencies which define the anisotropy of the trap $\lambda = \omega_r/\omega_z$ can be made so large that the Fermi energy E_F associated with the axial dynamics of the trap $N\hbar\omega_z$ and the temperature $k_B T$, are both much smaller than the energy level spacing of the radial confinement $\hbar\omega_r$ i.e., $N\hbar\omega_z, k_B T \ll \hbar\omega_r$ [7]. Due to extremely rarified nature of the gas, there are virtually no spin relaxation processes and the particles interact via s -wave scattering $g_{1D}\delta(z)$. Furthermore, in addition to the total number N , the total polarization of the cloud $P = (N_\uparrow - N_\downarrow)/(N_\uparrow + N_\downarrow)$ can also be varied through independent control of the number of particles in each spin projection N_σ . Formally this system is described by a Hamiltonian $\hat{H} = \int dz (H_0 + H_I)$ with :

$$\begin{aligned} H_0(z) &= \sum_{\sigma} \psi_{\sigma}^{\dagger} \left[-\frac{\hbar^2}{2m} \frac{\partial^2}{\partial z^2} + V_{\text{trap}}(z) - \mu_{\sigma} \right] \psi_{\sigma} \\ H_I(z) &= g_{1D} \psi_{\uparrow}^{\dagger}(z) \psi_{\downarrow}^{\dagger}(z) \psi_{\downarrow}(z) \psi_{\uparrow}(z) \end{aligned} \quad (1)$$

where $\psi_{\sigma}(z)$ and μ_{σ} represent the fermionic field operators and the chemical potential of atomic species with spin σ and $V_{\text{trap}}(z) = \frac{m}{2}\omega_z^2 z^2$. We define the Fermi energy, radius, momentum and temperature as $E_F = N$, $z_F = \sqrt{2E_F}$, $k_F = \sqrt{2E_F}$ and $T_F = E_F$ and measure the relative strength of the interaction with the ratio (γ) of the interaction (ϵ_I) and the kinetic (ϵ_k) energy densities. In the limit of weak interaction $\epsilon_I \sim g_{1D}\rho(z)$ and $\epsilon_k \sim \rho^2(z)$ yielding:

$$\gamma = g_{1D}/\rho \quad (2)$$

Our calculations are done using two methods with distinct but complementary advantages. First is the Time Evolving Block Decimation (TEBD) [23] (See Supplemental Material at for details of methods), an exact approach that retains all important correlations. Second is the mean-field Bogoliubov-de Gennes (BdG) method, an effective theory approach which retains only the two point correlations and describes the spin densities $\rho_{\sigma}(z)$

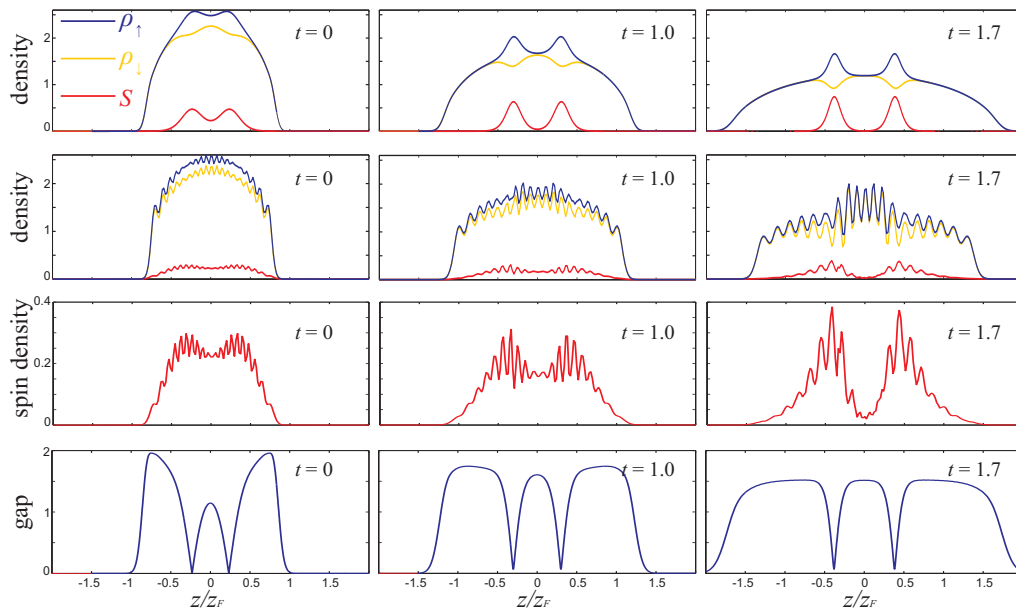


Figure 1: (color online) The expansion of sample with $N = 40$, $P = 0.05$ and $g_{1D} = -8.0$. From left to right, each column represents snapshots of the expansion dynamics at $t=0.0, 1.0, 1.7$ ($1/\omega_z$). Row 1 displays the density profiles. In each plot, we show ρ_\uparrow , ρ_\downarrow and $S = \rho_\uparrow - \rho_\downarrow$ obtained from BdG calculation. Row 2 is the same as Row 1 except that the results are obtained from TEBD calculation. Row 3 shows the spin densities $S(z)$ from the TEBD. Finally in Row 4 we plot the amplitude of the superfluid gap $|\Delta|$ from the BdG calculation.

and the superfluid gap $\Delta(z)$ through quasi-particle wavefunctions. The BdG has the advantage that, when correct, it provides a clear picture of the dynamics of the pairing field $\Delta(z) = g_{1D} \langle \psi_\uparrow(z) \psi_\downarrow(z) \rangle$ in direct association with the particle densities $\rho_\sigma(z) = \langle \psi_\sigma^\dagger(z) \psi_\sigma(z) \rangle$. However, although the BdG has been observed to give a very good description of 1D samples at weak interaction [10], we do not expect this trend to extend from moderate to strong interaction. On the other hand the TEBD method provides a stringent check for the observed phenomena in the BdG approach. In both cases we work at $T = 0$ and employ a canonical approach which fixes N and P .

To observe the FFLO state, experiments must verify crystalline order in $\Delta(z)$ or alternatively, that the average center-of-mass momentum of the pairs $\langle n_k \rangle$ is proportional to the separation of the Fermi surfaces $\langle n_k \rangle \propto k_\uparrow - k_\downarrow$. In 1D this relationship can be recast in terms of the spin density $S(z) = \rho_\uparrow(z) - \rho_\downarrow(z)$ as $\langle n_k \rangle \propto \pi \int_L S(z) dz / L$, where L is the size of the partially polarized region. Recently a number of authors [11, 12, 24] have suggested the measurement of the pair momentum distribution function n_k as the most promising avenue to detecting the finite center-of-mass momentum q of the pairs. These suggestions are extrapolations from equilibrium studies where n_k shows peaks at $k = \pm q$ in contrast to the peak at $k = 0$ expected for regular BCS pairing. However, we are not aware of analyses of n_k accounting for the interacting nature of the expansion dynamics and in particular how well this signal will be preserved. This is particularly important for 1D given

that γ increases during expansion [see Eq. (2)]. In this study we explore the possibility of finding a signal directly in real space. Our calculations reveal that:

- Upon axial expansion, strong accents develop in the spin density profiles.
- The position of these accents exactly coincide with the nodes in the pair correlation function and represent *prima facie* evidence of FFLO correlations.
- The strength of this signal increases with γ and decreases with polarization, being strongest when the spin excitations are gapped.
- The accents in the spin density move much more slowly than the edge of the cloud.

In Fig. 1 dramatic accents in the spin densities are observed as the expansion of the cloud proceeds. Through a comparison of the density plots with the corresponding gap parameter $|\Delta(z)|$ (bottom row in Fig. 1) one can make a key observation: *The position and growth of the spin density accents respectively coincide with the nodes and amplification of $|\Delta(z)|$.* Furthermore, these spin density accents (or the order parameter nodes) move much slower during the expansion compared to the edge of the whole cloud.

To understand this phenomenon, it is helpful to first layout some broad features of the ground state utilizing the phase diagram for a homogeneous system together with the local density approximation (LDA) [8, 9, 14].

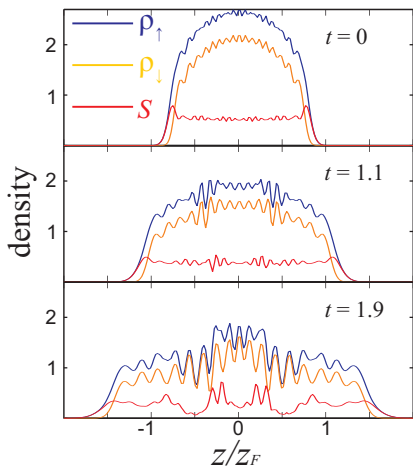


Figure 2: Density profiles, obtained from TEBD calculation, during the expansion of a sample with $N = 40$, $P = 0.15$ and $g_{1D} = -8.0$.

Under LDA, the trapped system can be regarded as locally homogeneous with chemical potential defined by: $\mu(z) = \mu_\sigma - V_{\text{trap}}(z)$. There are two regimes to be considered [7, 10, 11, 13, 14] depending on whether P is smaller or larger than a critical polarization P_c . For $P < P_c$, we obtain an FFLO state at the center of the trap surrounded by fully paired BCS wings at the edges. Here the BdG calculation tells us that there is exactly one excess spin bound to each of the nodes of the order parameter and the FFLO state is analogous to a band insulator of the *relative motion* between the unpaired and paired particles. The ground state represented in Fig. 1 is within this regime and density accents represent the localization of unpaired spins at the nodes of Δ . During the time of flight, the excess spins are kept pinned to the nodes of the order parameter and become more tightly bound. The dramatic effects observed occur when this localization couples with the average enhancement of $|\Delta|$ implied by an increasing γ as the density drops during expansion [see Eq. (2)]; a uniquely 1D phenomenon. Henceforth we refer to these accents as node signatures.

For $P > P_c$, the FFLO state still remains at the center in the ground state, but the wings exclusively contain the majority spin component. In this regime, there are more excess spins than nodes of Δ , and consequently they are less tightly bound. Here we expect the node signatures to be less dramatic which is confirmed in Fig. 2. In particular, the spin accents near the edges are not well resolved. We can therefore conclude that the best place to observe the node signature is at $P < P_c$ where the signal is enhanced by both a large separation of the nodes and greater contrast with the background density. We note that the value of P_c increases with $|g_{1D}|$ implying a sizable observation window at strong interactions where experiments are conducted.

At equilibrium the FFLO correlation appear as peaks

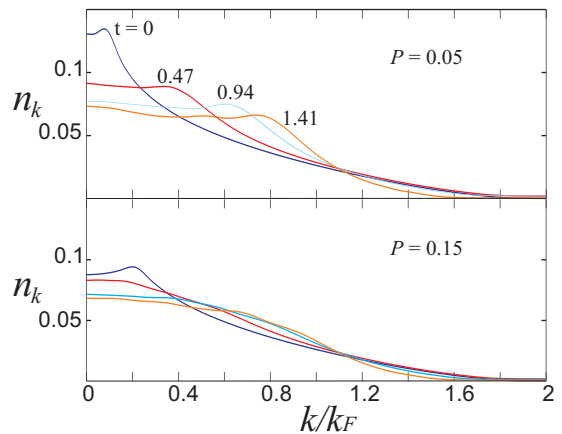


Figure 3: Pair momentum distribution at two different polarization for $g_{1D} = -8$ and $N = 40$. In each panel, we display n_k for different times. Counting from the left, the curves correspond to $t = 0, 0.47, 0.94$ and 1.41 , from top to bottom. In both cases the momentum peaks representing the FFLO state disappear from the plot during the expansion.

in the pair momentum distribution n_k defined by:

$$n_k = \frac{1}{L} \int \int dz dz' e^{ik(z-z')} O(z, z'), \quad (3)$$

where $O(z, z') \equiv \langle \psi_\uparrow^\dagger(z) \psi_\downarrow^\dagger(z) \psi_\downarrow(z') \psi_\uparrow(z') \rangle$ is the two-point correlation function. In Fig. 3 we observe the effects of interaction on this signature during the expansion. At sufficiently long time, n_k no longer possesses peaks at finite momentum.

One may wonder whether the node signatures can be observed in *in situ* density profiles of a trapped cloud with sufficiently large interaction strength. To answer this, we show in Fig. 4 the density profiles of a trapped system for $g_{1D} = -8, -20$ and -36 . (Note that for the experiment reported in Ref. [7], $g_{1D} \sim -50$ for the central tube.) One can see that the modulation depth of the spin density of a trapped cloud is not very sensitive to g_{1D} . This is in sharp contrast to the BdG calculation where the spin density modulation is indeed enhanced as γ is increased — an indication of the invalidity of the mean-field theory for strong interaction. In the exact calculation, the localization of excess spin at large $|g_{1D}|$ is counter-balanced by increased quantum fluctuations neglected in the mean-field theory. Therefore, the dramatic emergence of node signatures is a unique feature of expansion dynamics.

Finally, we address the question of the effect of the interaction strength in Fig. 5 where the spin densities in an expanding cloud are shown for two sets of interaction strength. Though the results from the strong and weak interaction are qualitatively similar, the spin accents start to develop earlier for the case of smaller g_{1D} . This could play an important role in practice when finite lifetime of the system must be taken into account.

In conclusion, we have investigated the expansion dy-

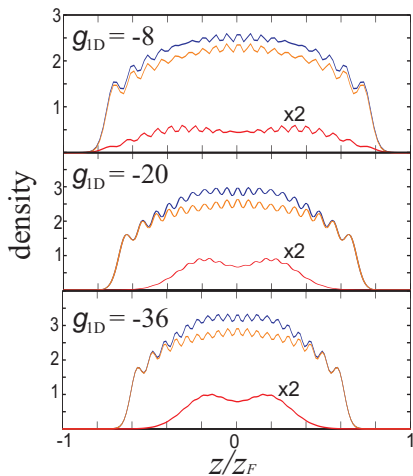


Figure 4: Ground state density profiles in trap, with $N = 40$, $P = 0.05$ and for different interaction strengths g_{1D} . In each plot, we show ρ_{\uparrow} , ρ_{\downarrow} and S obtained from TEBD calculation. For clarity, the spin density S is magnified by a factor of 2.

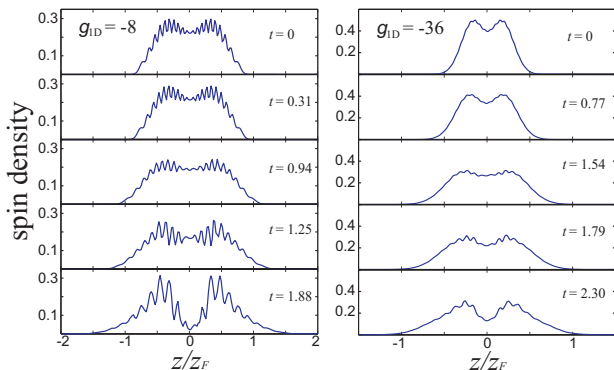


Figure 5: Expansion profiles for two different samples with $N = 40$, $P = 0.05$ but at different interaction strengths g_{1D} . In each plot, we plot the TEBD result for S . In both cases, the modulation depth of the spin density first reduces and then strengthens during expansion.

namics of polarized Fermi superfluid in 1D using both the BdG and TEBD methods. Our results predict that strong spin density modulations which can be readily observed in experiment, emerge during expansion and provide direct evidence of the FFLO state. Apart from the pair momentum distribution function described above, other methods [25] have been proposed in the literature to detect FFLO. However they all rely on interferometric techniques requiring two fermionic superfluids, one of them being the FFLO state. Our proposal, in contrast, only requires the FFLO cloud itself and hence is significantly simpler. In a more general context, our work shows that quantum dynamics of low-dimensional atomic gases is highly non-trivial and deserve a more thorough study in the future.

Part of the numerical calculations for this work was performed at NERSC, Navy DSRC, ARL, AFRL and the ARSC. We thank Eric Mueller, Randy Hulet, Micheal

Wall, Yean-an Liao and S. Bhongale for several illuminating discussions. This work is supported by the ARO Award W911NF-07-1-0464 with the funds from the DARPA OLE Programm, the Welch foundation (C-1669, C-1681) and the NSF.

-
- [1] P. Fulde, and R. A. Ferrell, Phys. Rev. **135**, A550 (1964).
 - [2] A. I. Larkin, and Y. N. Ovchinnikov, Zh. Eksp. Teor. Fiz. **47**, 1136 [Sov. Phys. JETP **20**, 762 (1965)].
 - [3] T. Mizushima, K. Machida, and M. Ichioka, Phys. Rev. Lett. **94**, 060404 (2005).
 - [4] A. M. Clogston, Phys. Rev. Lett. **9**, 266 (1962).
 - [5] B. S. Chandrasekhar, Appl. Phys. Lett. **1**, 7 (1962).
 - [6] R. Casalbuoni, and G. Nardulli, Rev. Mod. Phys. **76**, 263 (2004).
 - [7] Y.-A. Liao, A. S. Rittner, T. Paprotta, W. Li, G. B. Partridge, R. G. Hulet, S. K. Baur, and E. J. Mueller. Nature (London) **467**, 567 (2010).
 - [8] G. Orso, Phys. Rev. Lett. **98**, 070402 (2007).
 - [9] P. Kakashvili, and C. J. Bolech, Phys. Rev. A **79**, 041603 (2009).
 - [10] X. J. Liu, H. Hu, and P. Drummond, Phys. Rev. A **76** 043605, (2007).
 - [11] A. E. Feiguin, and F. Heidrich-Meisner, Phys. Rev. B **76** 220508(R), (2007).
 - [12] M. Casula, D. M. Ceperley, and E. J. Mueller, Phys. Rev. A **78**, 033607 (2008).
 - [13] M. M. Parish, S. K. Baur, E. J. Mueller, and D. Huse, Phys. Rev. Lett. **99**, 250403 (2007).
 - [14] M. Tezuka, and M. Ueda, New J. Phys. **12**, 055029 (2010).
 - [15] X. W. Guan, M. T. Batchelor, C. Lee, and M. Bortz, Phys. Rev. B **76**, 085120 (2007).
 - [16] J. Y. Lee, and X. W. Guan, Nucl. Phys. B **853**, 125 (2011).
 - [17] J. Kajala, F. Massel, and P. Torma, Phys. Rev. A **84**, 041601 (2011).
 - [18] M. W. Zwierlein, A. Schirotzek, C. H. Schunck, and W. Ketterle, Science **311**, 492 (2006).
 - [19] G. B. Partridge, W. Li, R. I. Kamar, Y.-A. Liao, and R. G. Hulet, Science **311**, 503 (2006).
 - [20] M. W. Zwierlein, C. H. Schunck, A. Schirotzek, and W. Ketterle, Nature(London) **442**, 54 (2006).
 - [21] S. Nascimbene, N. Navon, K. J. Jiang, L. Tarruell, M. Teichmann, J. McKeever, F. Chevy, and C. Salomon Phys. Rev. Lett. **103**, 170402 (2009).
 - [22] C. A. Regal, M. A. Greiner, and D. S. Jin, Phys. Rev. Lett. **92**, 040403 (2004).
 - [23] G. Vidal, Phys. Rev. Lett. **93**, 040502 (2004).
 - [24] K. Yang, Phys. Rev. Lett. **95**, 218903 (2005).
 - [25] V. Gritsev, E. Demler, and A. Polkovnikov, Phys. Rev. A **78**, 063624 (2008); H. Hu, and X.-J. Liu, Phys. Rev. A **83**, 013631 (2011); M. Swanson, Y. L. Loh, and N. Trivedi, arXiv:1106.3908.

METHODS - SUPPLEMENTARY MATERIAL

This system of $N = N_\uparrow + N_\downarrow$ is described by a Hamiltonian $\hat{H} = \int dz (H_0 + H_I)$ with non-interacting (H_0) and interaction (H_I) energy densities given by:

$$H_0(z) = \sum_\sigma \psi_\sigma^\dagger \left[-\frac{\hbar^2}{2m} \frac{\partial^2}{\partial z^2} + V_{\text{trap}}(z) - \mu_\sigma \right] \psi_\sigma,$$

$$H_I(z) = g_{1D} \psi(z) \psi_\downarrow^\dagger(z) \psi_\downarrow(z) \psi_\uparrow(z), \quad (4)$$

where $\psi_\sigma(z)$ represent the Fermionic field operators, m the mass and μ_σ the chemical potential of atomic species with spin σ . The 1D effective coupling constant $g_{1D} < 0$ is expressed through a relationship with the 3D scattering length a_{3D} by [1]: $g_{1D} = \frac{2\hbar^2 a_{3D}}{m a_l (1 - A a_{3D} / a_l)}$. Here a_l is the oscillator length and $A = \xi(1/2)/\sqrt{2}$. We work in 'trap' units: $m = \omega_z = \hbar = k_B = 1$.

BdG Calculation

We treat \hat{H} within the mean-field Bogoliubov-de Gennes (BdG) approach for which there are many excellent references [2]. Here we simply state the BdG equations for the pair wave functions $u_j(z)$ and $v_j(z)$ which decouple \hat{H} :

$$\begin{bmatrix} H_\uparrow^S - \mu_\uparrow & \Delta(z) \\ \Delta(z) & -H_\downarrow^S + \mu_\downarrow \end{bmatrix} \begin{bmatrix} u_j \\ v_j \end{bmatrix} = E_j \begin{bmatrix} u_j \\ v_j \end{bmatrix}, \quad (5)$$

where E_j is the associated energy. Despite this, the BdG treatment has been shown to yield qualitatively reliable answers [2]. In accordance with Fermionic commutation relations, the quasi-particle amplitudes are normalized as: $\int dz |u_j(z)|^2 + |v_j(z)|^2 = 1$. In terms of which the Gap $\Delta(z)$ and the free energy Ω , may be written as:

$$\Delta(z) = U \sum_{j=1}^{\infty} u_j(z) v_j^*(z) f(E_j), \quad (6)$$

where $f(E)$ represents the Fermi-Dirac distribution function: $f(E) = 1/(e^{E/k_B T} + 1)$. We follow a convention that $N_\uparrow > N_\downarrow$, we define $k_F^{\uparrow\downarrow} = \sqrt{2\mu_{\uparrow\downarrow}}$ and the FFLO wave number by $q_0 = k_F^\uparrow - k_F^\downarrow$.

Our theoretical framework is encapsulated within Eqs. (5) and (6) and we discretize the system of Eq. (5) using a piece-wise linear finite element basis which ensures the continuity of both $u(z)$ and $v(z)$. A reduction of Eq. (5) into even and odd parity states about $z = 0$ is possible due to anticipated reflection symmetry of Δ about this axis. Nevertheless, each independent sub-block with distinct parity presents a very large eigenvalue problem because of the slow convergence of Eq. (6). The slow convergence is tackled using a hybrid BdG-semi-classical strategy similar to Ref. [2]. Starting from an initial state

Eq. (5) is iteratively solved to self-consistency using the modified Broyden's method [3]. We work in a canonical formalism which keeps N and the total polarization $P = (N_\uparrow - N_\downarrow)/N$ fixed through the number equations $N_\sigma = \int dz \rho_\sigma(z)$.

TEBD calculations

To implement TEBD formalism, we employ a 1D Fermi-Hubbard Hamiltonian to approximate the continuum quasi-1D polarized Fermi gases in harmonic traps:

$$H = -J \sum_\sigma \sum_{i=2}^L (c_{i,\sigma}^\dagger c_{i-1,\sigma} + h.c.) + U \sum_{i=1}^L n_{i,\uparrow} n_{i,\downarrow} + \sum_{i=1}^L V_i (n_{i,\uparrow} + n_{i,\downarrow}), \quad (7)$$

where L is the number of discretized lattice sites, $c_{i,\sigma}^\dagger, c_{i,\sigma}$ are respectively the creation and annihilation operators for spin σ particles at i th lattice site, J is the hopping amplitude between the neighboring sites, and U is the on-site interaction strength between two unlike spins. The connection between the Fermi-Hubbard Hamiltonian (7) and the Hamiltonian (4) upon which the BdG calculation is based can be seen as follows: In the trap units we mentioned above, the hopping amplitude $J = \frac{L^2}{2l^2}$, where l is the total length of system (in our dimensionless units). From these, the parameters $\frac{U}{J} = 2g_{1D}l/L$ and $\frac{V_i}{J} = (\frac{l}{L})^4 (i - \frac{L}{2})^2$ are chosen accordingly. In our calculation, typically we choose $L = 300 \sim 400$. With these properly chosen characteristic parameters, the discretized Hubbard Hamiltonian can be trusted to represent a continuum system as have been previously shown [4].

The TEBD algorithm utilizes the Schmidt decomposition and the convergence of the simulation is mainly controlled by the so-called Schmidt rank χ , which is the number of eigenvalues retained when truncating the Hilbert space. In our calculation, since the computation time scales as χ^3 , the optimal value of $\chi \sim 100 - 150$ is chosen to ensure the convergence is good enough when comparing with the results with higher χ . Another source of error comes from the Trotter-Suzuki expansion for the time evolution operator. To reduce it, we adopt fifth order Trotter-Suzuki expansion in our calculation while choosing a small enough time step based on self-consistent stability test.

-
- [1] T. Bergeman, M. G. Moore, and M. Olshanii, Phys. Rev. Lett. **91**, 163201 (2003).
 - [2] Xia-Ji Liu, Hui Hu, and Peter Drummond, Phys. Rev. A **75** 023614, (2007).
 - [3] D. D. Johnson, Phys. Rev. B. **38**, 12807 (1988).

[4] M. Tezuka, and M. Ueda *New J. Phys.* **12**, 055029 (2010).